

Response of the tropical Pacific Ocean to El Niño versus global warming

Fukai Liu¹ · Yiyong Luo¹ · Jian Lu² · Xiuquan Wan¹

Received: 6 August 2015 / Accepted: 3 April 2016 / Published online: 15 April 2016
© Springer-Verlag Berlin Heidelberg 2016

Abstract Climate models project an El Niño-like SST response in the tropical Pacific Ocean to global warming (GW). By employing the Community Earth System Model and applying an overriding technique to its ocean component, Parallel Ocean Program version 2, this study investigates the similarity and difference of formation mechanism for the changes in the tropical Pacific Ocean under El Niño and GW. Results show that, despite sharing some similarities between the two scenarios, there are many significant distinctions between GW and El Niño: (1) the phase locking of the seasonal cycle reduction is more notable under GW compared with El Niño, implying more extreme El Niño events in the future; (2) in contrast to the penetration of the equatorial subsurface temperature anomaly that appears to propagate in the form of an oceanic equatorial upwelling Kelvin wave during El Niño, the GW-induced subsurface temperature anomaly manifest in the form of off-equatorial upwelling Rossby waves; (3) while significant across-equator northward heat transport (NHT) is induced by the wind stress anomalies associated with El Niño, little NHT is found at the equator due to a symmetric change in the shallow meridional overturning circulation that appears to be weakened in both North and South Pacific under GW; and (4) heat budget analysis shows that the maintaining mechanisms for the eastern equatorial Pacific warming are also substantially different.

Keywords Tropical Pacific Ocean · Global warming · El Niño · El Niño-like response

1 Introduction

El Niño–Southern Oscillation (ENSO) is the leading mode of the interannual variability in the Earth’s climate system and has significant impacts on climate variability across much of the globe. The warm phase of ENSO, or El Niño, is characterized by an anomalously warm ocean temperature in the central and eastern equatorial Pacific (CEP), accompanying with an eastward shift of the warm pool and rainfall, a reduction of the equatorial easterly winds, and a flattening of the zonal thermocline slope (Rasmusson and Carpenter 1982; Neelin et al. 1998; Wang and McPhaden 2000, 2001). Ocean–atmosphere coupling is a major cause of ENSO (Bjerknes 1969; Zebiak and Cane 1987), and the thermocline–SST positive feedback (i.e., the Bjerknes feedback) is believed to be responsible for the onset and strengthening of El Niño. For the termination of El Niño or its transition to the cold phase (i.e., La Niña), four negative feedbacks have been proposed: the delayed oscillator (Suarez and Schopf 1988; Battisti 1988), discharge–recharge oscillator (Jin 1996, 1997a, b), western Pacific oscillator (Wang and Weisberg 1994; Weisberg and Wang 1997), and advective–reflective oscillator (Picaut et al. 1996, 1997). Due to the complexity of the evolution of ENSO, more than one of the above negative feedbacks may be operating in a variety of combinations (Wang and Picaut 2004).

On the other hand, a majority of climate models (e.g., Knutson and Manabe 1995; Liu et al. 2005; Held and Soden 2006; Xie et al. 2010; Lu and Zhao 2012) has projected that the mean climate condition in the tropical Pacific Ocean shifts towards an ‘El Niño-like’ state (Zhang et al.

✉ Yiyong Luo
yiyongluo@ouc.edu.cn

¹ Physical Oceanography Laboratory, Ocean University of China, 238 Songling Road, Qingdao 266100, China

² Atmospheric Sciences and Global Change Division, Pacific Northwest National Laboratory, Richland, WA, USA

1997) under global warming (GW), with features such as an enhanced warming in the east, a shoaling of the thermocline in the western equatorial Pacific (WEP), and a weakening of the south equatorial current (SEC). These oceanic changes are generally interpreted as a direct response to a weakening of easterly wind anomalies in the equatorial Pacific associated with the slowdown of the Walker circulation, a robust signature of the atmospheric response to GW (e.g., Vecchi and Soden 2007). However, it has been found that the physical mechanisms that drive tropical Pacific climate change depart substantially from the ENSO analogy (DiNezio et al. 2009). Recently, Luo et al. (2015) demonstrated that the weakening of the equatorial easterlies contributes only marginally to the El Niño-like SST warming pattern under GW, and this warming pattern appears to be mainly controlled by the air-sea thermal interaction. Their model experiments revealed further differences between the El Niño-like response to GW and El Niño: although in both cases the upwelling in the CEP weakens, the total effect of vertical advection in the mixed layer is opposite, cooling for GW (due to enhanced upper-ocean stratification) but heating for El Niño.

Since the shift of mean climate conditions toward the ‘El Niño-like’ state could alter the amplitude, frequency, seasonal timing or spatial patterns of ENSO and then affect a range of weather phenomena (Collins et al. 2010; Vecchi and Wittenberg 2010; DiNezio et al. 2012), it is of great importance to understand the differences and similarities of underlying formation mechanisms for the tropical Pacific between GW and El Niño. However, it is still debatable as to whether ENSO activity will be weakened or strengthened, owing to the delicate balance of competing processes under GW. For example, an enhanced thermal stratification and associated shallower thermocline along the equatorial Pacific tends to destabilize the tropical coupling system, increase the sensitivity of SST to an anomaly in thermocline or wind stress, and thus increase the amplitude of ENSO; on the other hand, the higher Newtonian damping on the SST (Xie et al. 2010) and more stable atmosphere due to a less vigorous zonal circulation tend to reduce the amplitude of ENSO (Philip and Oldenborgh 2006; Zhang et al. 2008).

These existing studies above focused mainly on the annual mean state differences between GW and El Niño, and little attention has been given to their different seasonalities. The seasonal cycle can contribute to the irregularity and phase locking of ENSO, and the intra-seasonal variability can be a source of both ENSO variability and irregularity (Wang and Picaut 2004). In addition, the seasonal cycle is responsible for around 90 % of the total surface temperature variance on annual and longer time scales (Dwyer et al. 2012). In this study we investigate the similarity and difference of the SST formation processes

between GW and El Niño, with a focus on their seasonal evolution. To this end, we conducted a suite of numerical experiments using the NCAR’s Community Earth System Model version 1.1 (CESM1.1) and its ocean component, the Parallel Ocean Program version 2 (POP2). In particular, an overriding technique is employed as a diagnostic tool to isolate and evaluate the role of wind changes in the robust features of the tropical Pacific Ocean under GW versus El Niño. The overriding technique enables us to isolate individual feedbacks (e.g., the wind-thermocline-SST feedback) from other factors (Lu and Zhao 2012; Luo et al. 2015). In addition, a heat budget analysis will be performed to further diagnose the mechanisms of the SST formation under GW versus El Niño.

The rest of the paper is structured as follows. The model and numerical experiments are described in the next section. In Sect. 3, the methods used to calculate energy budget and construct an El Niño composite are explained. In Sect. 4, we compare the oceanic and atmospheric changes over the tropical Pacific between GW and El Niño, including mean patterns, seasonal evolutions, subsurface changes and northward heat transports. The results of heat budget analysis are presented in Sect. 5. Finally, a summary and a discussion of our findings are given in Sect. 6.

2 Model and experiment design

The main modeling tool for this study is CESM1.1, which is comprised of the Community Atmospheric Model version 5 (CAM5), the Community Land Model version 4 (CLM4) and the POP2 ocean component. The horizontal resolution of CAM5 and CLM4 is 1.9° longitude \times 1.9° latitude, with the atmospheric component having 30 vertical levels. The horizontal resolution of the POP2 is nominal 1° , telescoped meridionally to $\sim 0.3^\circ$ at the equator. Vertically, it has 60 uneven levels with the thickness varying from 10 m near the surface to 250 m near the bottom.

Initialized from the end of the historical experiment (1861–2005) available at NCAR, we conduct a 94-year projection run under the Representative Concentration Pathway (RCP) 8.5 scenario from 2006 to 2099 using CESM1.1, and save its daily outputs of various atmospheric forcing variables. This experiment is labeled “CPL85” (Table 1). GW-induced linear trends are derived from least-squared linear fitting from this experiment. In addition, the data from the CPL85 simulation will be used to construct an El Niño composite, the procedure for which will be explained in details in Sect. 3.

Applying the daily surface atmospheric forcing fields (including winds, air temperature, air pressure, specific humidity, precipitation rate, air density, and net short-wave and downward long-wave radiations) from CPL85, the

Table 1 Experiments with CESM1.1 and POP2

Name	Run (years)	Description
CPL85	94	RCP8.5 simulation with NCAR's Community Earth System Model from 2006 to 2099
FULL	94	POP2 is integrated from 2006 to 2099 with daily wind stress and fluxes from CESM
CTRL	94	POP2 is forced repeatedly by the 2006 daily wind stress and fluxes from CESM
STRS	94	Same as FULL, but wind stress is specified to that of 2006
SPED	94	Same as FULL, but wind speed is specified to that of 2006 through bulk formula
WIND	94	Same as FULL, but both wind stress and wind speed are specified to those of 2006

POP2 is then integrated for 94 years from 2006 to 2099, and this experiment is called “FULL” (Table 1). Note that bulk formulae are used to calculate the latent and sensible heat fluxes as the thermal forcing for the POP2. A comparison of the SST trend in the tropics between CPL85 and FULL demonstrates that the signature of the SST response in CPL85 is well reproduced by FULL, including an ‘El Niño-like’ warming pattern in the tropical Pacific Ocean (see Fig. 2 of Luo et al. 2015). As we are aware of that the way how the ocean interacts with the atmosphere is changed in the ocean-alone experiments and this might introduce a shock at year 2006 and an artificial trend as a result of the adjustment to the shock, we conduct another experiment with POP2 driven periodically by the same atmospheric fields of year 2006 for 94 years. This experiment serves as the control run for the overriding experiments and is referred to as CTRL (Table 1).

In order to isolate the effect of changing wind stress (wind speed), experiment STRS (SPED) is performed with the wind stress (wind speed) fixed at periodical annual cycle of year 2006 while all other fields being the same as FULL. The wind stress contribution to the oceanic changes can be derived by subtracting STRS from FULL, and the wind speed contribution by subtracting SPED from FULL. The former reflects the effect of wind stress change on the ocean circulation and then the thermal structure (over the CEP region, it refers to the effect of wind stress change on SST through the Bjerknes feedback). The latter reflects the effect of wind speed change on the latent heat flux through evaporation (referred to as Wind–Evaporation–SST or WES effect hereafter). It should be stressed that this WES effect only accounts for the direct thermal effect on ocean of the changing wind speed, not including the indirect feedbacks through the atmospheric processes as the WES in the fully coupled model (Lu and Zhao 2012). The experiment WIND with both wind stress and wind speed fixed at year 2006 values is conducted to assess the linearity of the oceanic response to the two aspects to wind forcing, which turns out to hold accurately. In addition, the effect of warming in the absence of wind stress and wind speed changes can be derived by subtracting CTRL from WIND, hereafter referred to as thermal warming (TW) effect.

The TW includes the feedbacks from both ocean dynamics (associated with the heat convergence due to the mean ocean circulation) and the atmospheric processes other than the wind stress and wind speed (such as the sensible heat flux and cloud radiative flux), with the latter taking a more effective role in shaping pattern of the tropical SST according to our previous work (Luo et al. 2015).

In brief, the wind stress effect (WS) can be deduced from FULL to STRS, the wind speed effect (WES) from FULL to SPED, and the TW effect from WIND to CTRL. FULL–CTRL mimics the full response in the coupled CESM1.1, encompassing all the effects above. Our analysis is based on monthly mean fields, and all El Niño-induced anomalies are computed with respect to each experiment's own climatology while the GW-induced changes are the linear trends over 2006–2099 periods.

3 Methods of analysis

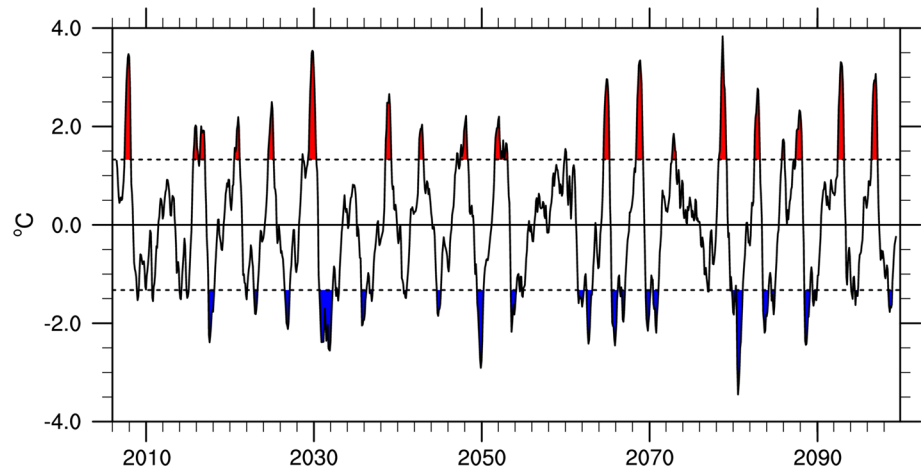
3.1 Temperature budget equation

It has been a common practice to use an upper layer with a flat bottom to diagnose the SST evolution (DiNezio et al. 2009, 2012; Alory and Meyers 2009), and the 0–55 m layer temperature (referred to as mixed layer temperature, MLT, hereafter) has very similar interannual variability (not shown) to the SST in our experiments. Therefore, we perform a temperature budget analysis with constant depth 55 m following the method in DiNezio et al. (2009) to diagnose the leading maintaining mechanisms for the SST anomalies revealed by the experiments. The temperature budget analysis is based on the vertical integration between 55 m depth and the surface of the temperature equation:

$$T_t = H - uT_x - vT_y - wT_z + T_{diff} \quad (1)$$

where T_t represents the tendency of the MLT; $H = (Q_0 - Q_h)/(\rho_0 c_p h)$ is the net heat flux, in which Q_0 and Q_h are the heat fluxes at the surface and heat penetration at the water depth of 55 m, respectively, ρ_0 and c_p are the density and specific heat of sea water; $-uT_x$, $-vT_y$, and $-wT_z$ are the zonal, meridional, and vertical

Fig. 1 Monthly MLT anomaly (relative to a base period climatology from 2006 to 2099) at Niño3.4 region (120°W–170°W and 5°S–5°N) smoothed with a 3-month running-mean filter. 18 El Niño events are identified during the 94-year simulation period based on the threshold that the MLT anomaly exceeds one standard deviation (1.3 °C, horizontal dashed line) for a minimum of three consecutive months



advection, respectively; and T_{diff} represents the ocean heat transport by unresolved processes and will be referred to as diffusion term hereafter. A positive (negative) T_{diff} indicates a heating (cooling) effect by diffusion. Ideally these unresolved processes in the temperature equation can be analyzed to close the heat budget. However, since only monthly oceanic outputs are saved and the diffusion terms are not stored as part of the model's outputs, the ocean heat transport by unresolved processes and submonthly oceanic processes can be only inferred as a residual from Eq. (1). Similar practice is common for analyzing the heat budget using the CMIP3 and CMIP5 dataset (e.g., DiNezio et al. 2009).

3.2 El Niño composite

We construct an El Niño composite following the procedure of Deser et al. (2012). After the simulated time series from 2006 to 2099 in CPL85 are detrended to remove the GW signal, the MLT anomaly over the Niño3.4 region (170°W–120°W, 5°S–5°N) are obtained. In this analysis, we identify 18 El Niño events based on the threshold that the 3-month-running-averaged MLT anomalies in Niño 3.4 exceed one standard deviation for a minimum of three consecutive months (Fig. 1). Figure 2a shows the seasonal evolution of their composite. The composite reaches its peak during the boreal winter of year 0 and its magnitude is consistent with observations (e.g., Rasmusson and Carpenter 1982). For convenience of discussion, we divide the evolution of El Niño into four different stages: (a) the development phase extending from Jan. to May of year 0; (b) the peak phase from Jul. to Dec. of year 0; (c) the decay phase from Jan. to Jun. of year 1; (d) the demise phase from Jul. to Dec. of year 1. In addition, to facilitate the comparison between El Niño and GW, we define a 12-month “El Niño year” to be the average from July of year 0 to June of year 1, thus the annual mean state of El Niño can be compared

with that of GW. As will be shown in Sect. 4, the composite El Niño captures well the major characteristics of the observed El Niño.

As the experiment of FULL-CTRL reproduces faithfully the interannual variability of CPL85, we use the same 18 events as in CPL85 for the El Niño composite for the overriding experiments. It is found that the evolution of the El Niño composite in CPL85 (Fig. 2a) is well reproduced by FULL-CTRL (Fig. 2b), but with a slightly larger amplitude, the reason of which will be left for future investigation. The WS effect plays a dominant role in the El Niño evolution (Fig. 2c), while the contribution from the WES effect is negligible (Fig. 2d). Interestingly, in the absence of the wind stress and wind speed changes, the TW effect can also produce weak El Niño events (Fig. 2e), consistent with the notion of Clement et al. (2011) that an El Niño-like spatial structure in the equatorial Pacific may develop in the absence of Bjerknes feedback.

The analysis in the following sections is based primarily on the CPL85 simulation, and the overriding experiments will be used to further isolate the role of individual feedbacks in the formation of El Niño and GW. Due to the high similarities between CPL85 and FULL-CTRL, all the discussions related to the CPL85 run can be carried over to FULL-CTRL. Besides, since the magnitude of the modeled WES-induced oceanic change is negligible during both El Niño (Fig. 2d) and GW (Luo et al. 2015) based on our analysis, we will not show the results of FULL-SPED (WES feedback) in the rest of this paper.

To facilitate the comparison of the SST pattern with El Niño, the basin mean warming (averaged over 10°S–10°N in the Pacific Ocean) in GW is first removed and the resultant anomalies are then rescaled to have a maximum of 3 °C—the maximum MLT anomaly of El Niño. In so doing, MLT warming less than the basin mean warming is represented by a cooling in Figs. 3b, 4b and 5b. Note the rescaling is only applied to GW-induced

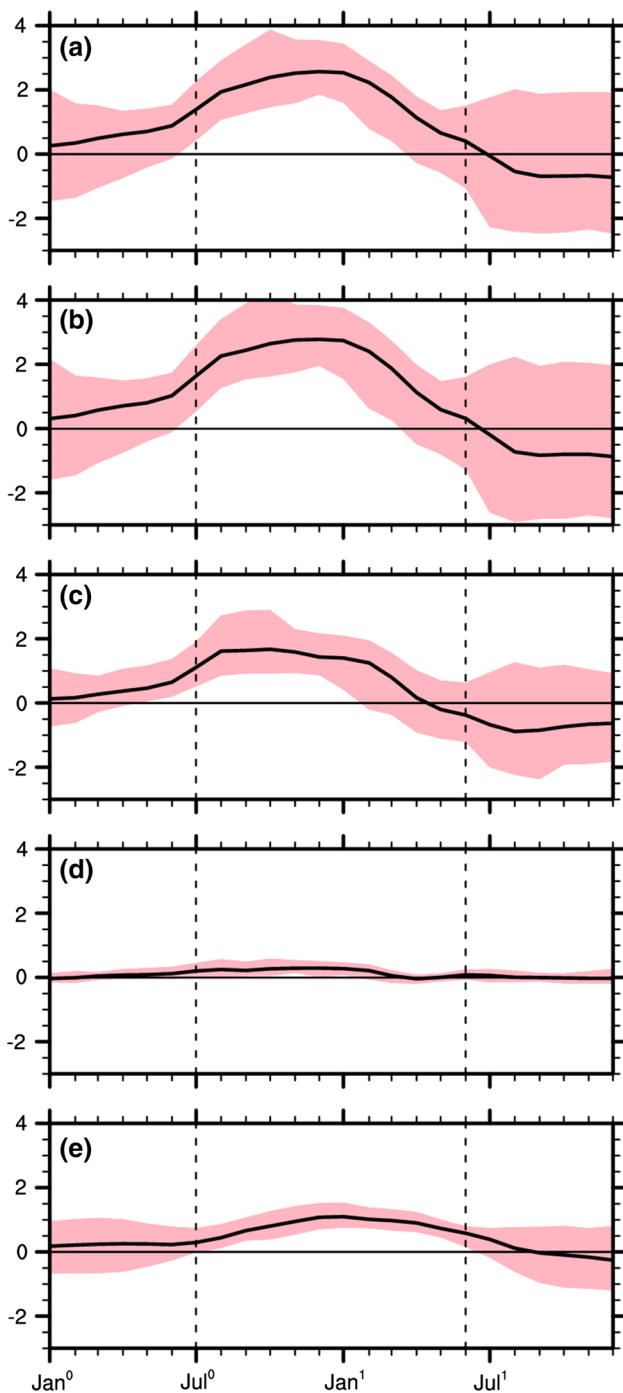


Fig. 2 Seasonal evolution of the El Niño composite at Niño3.4 region **a** CPL85, **b** FULL-CTRL (full response), **c** FULL-STRS (wind stress effect), **d** FULL-SPED (wind speed effect), **e** WIND-CTRL (thermal warming effect). Pink area denotes the upper and lower limits of the 18 composite members

MLT anomalies (i.e., Figs. 3b, 4b, 5b), and the temperature anomalies along the equator on the right panels of Fig. 6 are original values.

4 Oceanic and atmospheric changes in the tropical Pacific

4.1 Mean patterns

Various features of the El Niño composite are shown on the left panels of Fig. 3. In comparison with observations (e.g. Rasmusson and Carpenter 1982; Wang and McPhaden 2000, 2001), CESM shows considerable realism in simulating the El Niño spatial distributions over the tropical Pacific. Warm MLT anomalies appears in the CEP with maximum warming $\sim 3^\circ\text{C}$ around 105°W (Fig. 3a), accompanied by easterly wind anomalies (Fig. 3c) in the central equator as well as less net heat flux over the CEP (Fig. 9g). The oceanic changes also include a shoaling of the thermocline in the east but a deepening in the west (Fig. 6i), a slowdown of the Tropical Cells (TCs) (Fig. 8a) and a reduction of the upwelling along the equator (Fig. 3g). In addition, the westward SEC is found to strengthen over the east (Fig. 3e), which is arisen from a stronger local easterly (Fig. 3c). In the eastern equatorial region, another signature of change is a significant reduction of the upper-ocean stratification (Fig. 3i) due to a deepening of the thermocline there (Fig. 6i).

GW-induced changes are shown on the right panels of Fig. 3. The MLT exhibits a clear El Niño-like pattern in the tropical Pacific (Fig. 3b), with enhanced warming in the central and eastern equator and less warming in the west. The differences between the GW pattern and that of the El Niño are also salient. For example, the El Niño warming extends to $\pm 15^\circ$ latitude (Fig. 3a), and displays a greater symmetry about the equator than the GW pattern. For the latter, however, there is a pronounced cooling (lack of warming) in the southeastern tropical Pacific, which has no counterpart in the northern tropical Pacific. This asymmetry has been suggested to root in the asymmetry of the pattern of the change of the trade winds (see Fig. 3d) through the WES feedback (Xie et al. 2010; Lu and Zhao 2012; Luo et al. 2015).

In addition, the westerly anomalies along the equator under GW are found to shift eastward in comparison with those during El Niño (compared Fig. 3d–c), with the center of the anomalies around 120°W in the former but around 160°W in the latter. The zonal shift of the wind stress plays a decisive role in the oceanic anomalous patterns along the equator (An and Wang 2000). For example, in response to the shift of the weakened easterlies, GW induces a weakening of the SEC in the eastern equatorial region, in contrast to its strengthening there during El Niño (comparing Fig. 3f–e).

The most striking difference between GW and El Niño may be the upper-ocean stratification in the CEP, which is

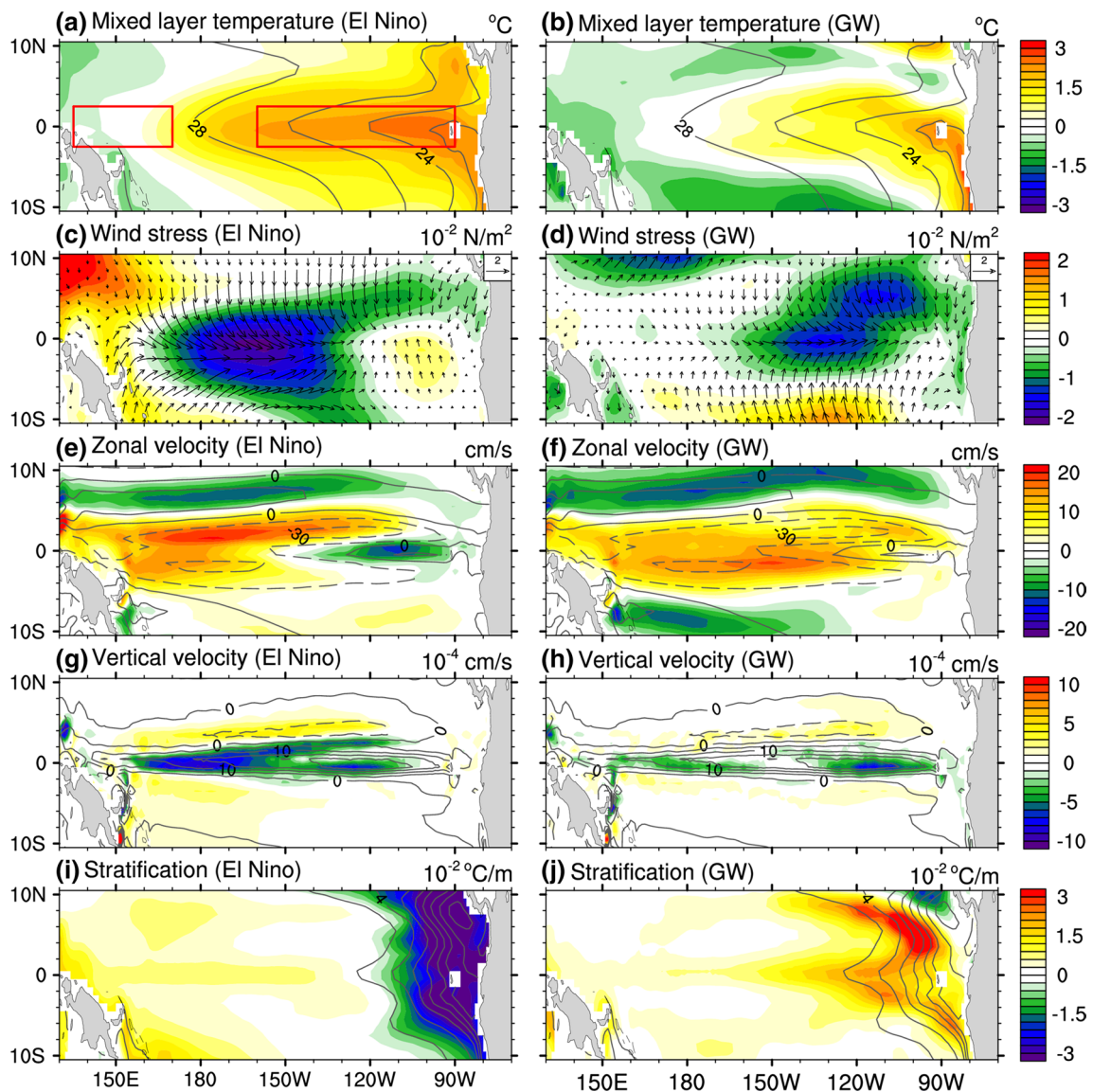


Fig. 3 The El Niño- (left) and GW-induced (right) changes (shading) and their corresponding climatological fields (contours) in the “El Niño year”: **a, b** MLT, **c, d** wind stress and its magnitude, **e, f** zonal velocity averaged over the top 55 m, **g, h** vertical velocity at depth of 50 m, and **i, j** mixed layer stratification. The GW-induced changes are their trends over 2006–2099 normalized by multiplying

100 years, and the MLT in **(b)** is further normalized by subtracting the mean value of field over 10°S–10°N in the Pacific Ocean and then rescaled to correspond to a 3 °C increase. The boxes in **(a)** represent the WEP (2.5°S–2.5°N, 135°E–170°E) and the CEP (2.5°S–2.5°N, 160°W–90°W) regions, respectively

enhanced under GW (Fig. 3j) but weakened under El Niño (Fig. 3i). The overriding experiments reveal that the weakening of the stratification during El Niño is due mainly to the WS effect (Fig. 5c), in agreement with previous studies (Rasmusson and Carpenter 1982; Neelin et al. 1998; Wang and McPhaden 2000, 2001). Under GW, however, both the WS and the TW effects appear to be responsible for the enhanced stratification (Fig. 5d). More specifically, during El Niño, the weaker-than-normal easterlies along the equator deepen the thermocline and induce larger warming in the subsurface than surface in the CEP (Fig. 6i),

thus reducing the temperature gradient in the vertical there. However, the GW scenario produces a more stratified upper layer due to an ocean warming that is greater near the surface and decreasing with depth (Fig. 6j) (Luo et al. 2009). These changes in stratification will be further discussed together with the vertical velocity change in Sect. 5.

4.2 Seasonal evolution

The seasonal evolutions of the MLT and the related circulation features along the equator are shown in Fig. 4 for

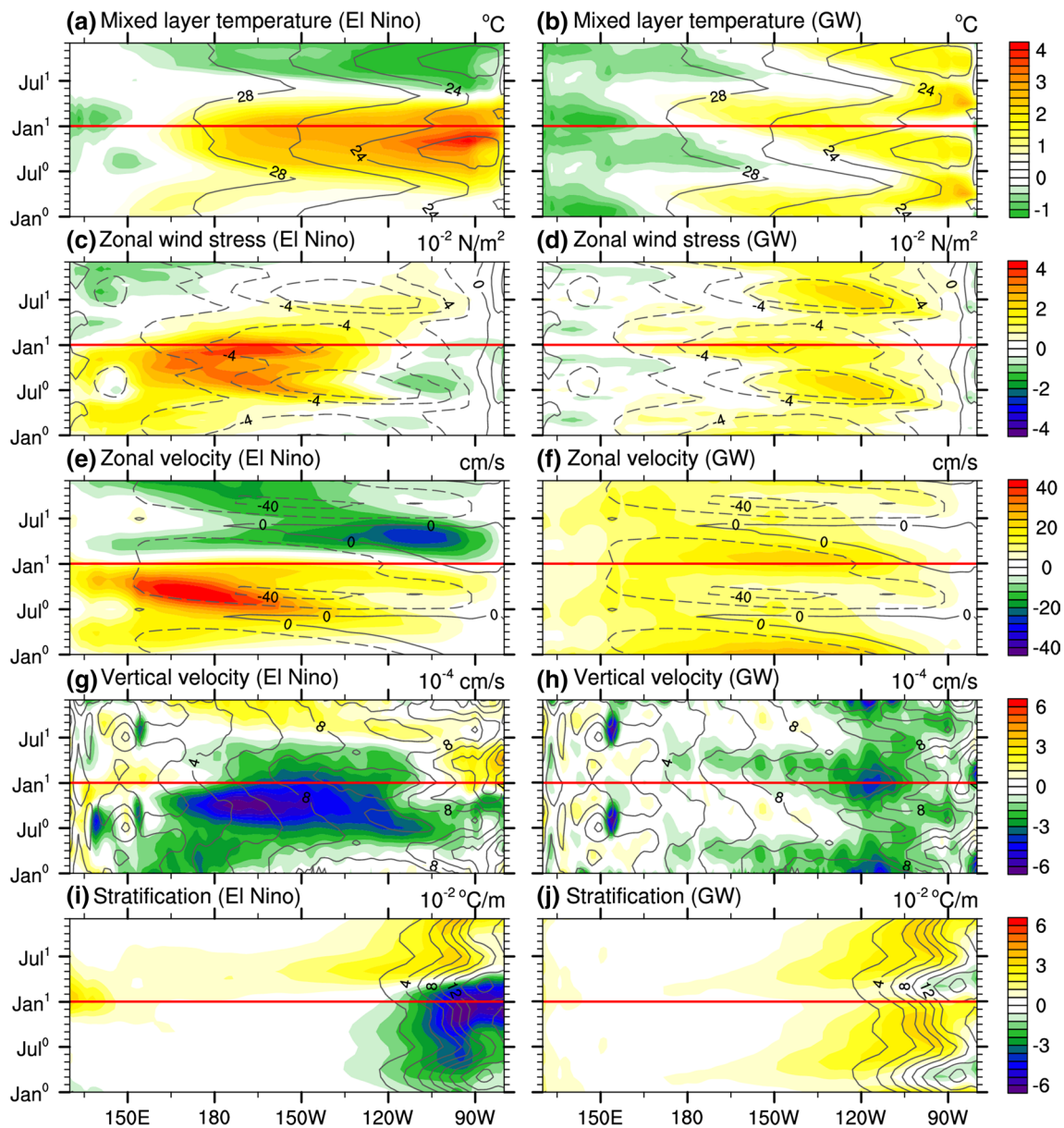


Fig. 4 Seasonal evolution of anomalies (*shading*) and their corresponding climatological fields (*contours*) during the El Niño composite (*left*) and GW (*right*) along the equator (averaged between 2.5°S and 2.5°N): **a, b** MLT, **c, d** zonal wind stress, **e, f** zonal velocity aver-

aged over top 55 m layers, **g, h** vertical velocity at depth of 50 m, and **i, j** mixed layer stratification. The anomalies under GW are their trends over 2006–2099 normalized by multiplying 100 years

El Niño and GW, respectively. As in the observations and previous modeling studies (e.g. Zhang et al. 2007; Huang et al. 2010, 2012), during El Niño, westerly anomalies start to build up west of dateline in the El Niño development phase, propagate eastward and strengthen in the following months, and then reach the peak magnitude around Dec. of year 0 (Fig. 4c). In company with the evolution of the wind anomalies, the oceanic responses include an enhanced MLT warming (Fig. 4a), a reduction of the SEC (Fig. 4e), and a weakening of both upwelling (Fig. 4g)

and upper-ocean stratification (Fig. 4i) during the El Niño development phase, and these changes reach their maxima around the peak phase of El Niño. These are followed by a delayed basin warming of the Indian Ocean, that forces a baroclinic atmospheric Kelvin wave into the western Pacific, causing the transition from the anomalous westerly winds to easterly winds over the WEP (e.g., Okumura et al. 2011; Wang and McPhaden 2000; Wang and Zhang 2002). The gradual weakening of the dominant westerly anomalies along the equatorial Pacific leads to the transition from

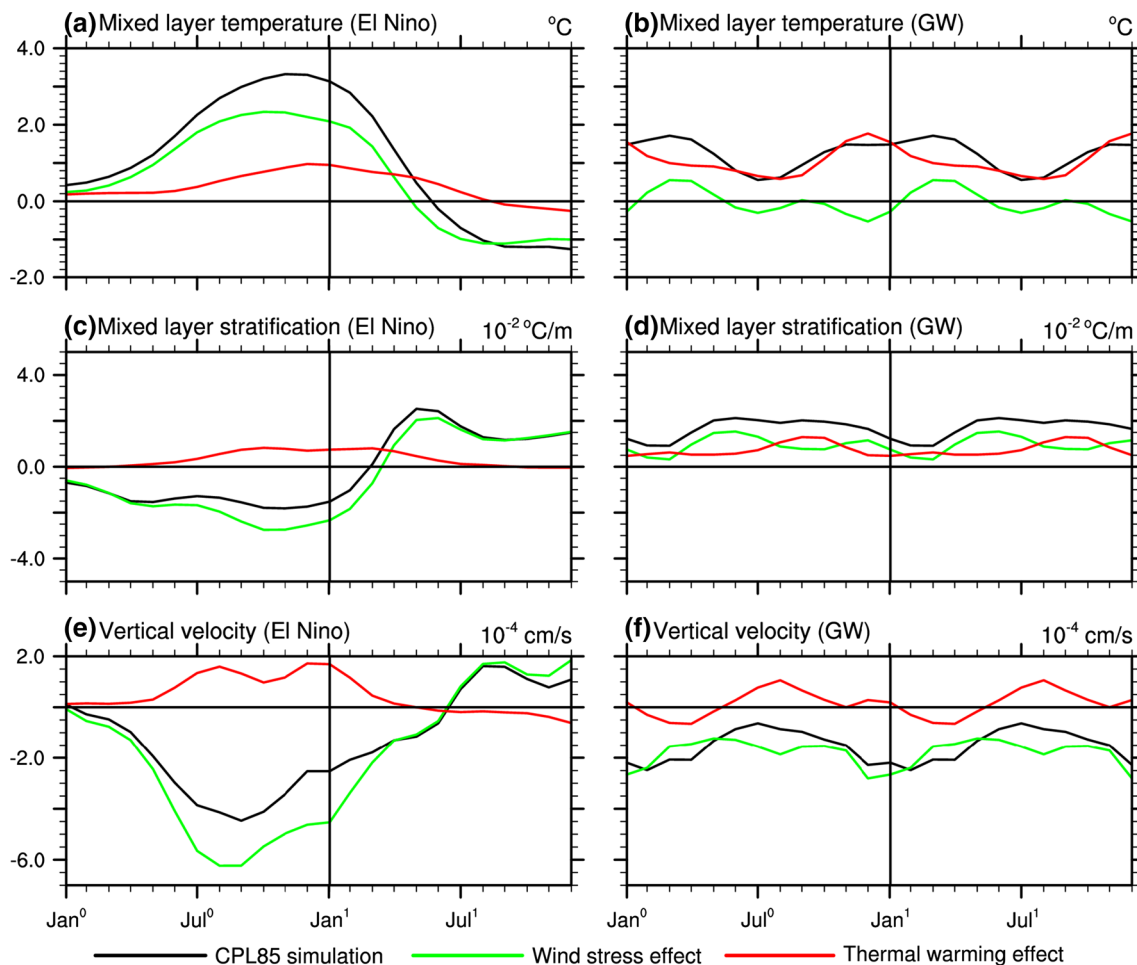


Fig. 5 The El Niño- (*left*) and GW-induced (*right*) changes in **a, b** MLT, **c, d** mixed layer stratification, and **e, f** vertical velocity at depth of 50 m over the CEP in CPL85 simulation (*black*), wind stress effect

(FULL-STRS) (*green*), and the thermal warming effect (WIND-CTRL) (*red*)

El Niño to La Niña during year 1. The major contribution of the wind changes during El Niño described above is further confirmed by the results of our overriding experiments (Fig. 5a), that is, the WS effect plays an important role for the magnitude as well as seasonal evolution of MLT anomaly over the equatorial Pacific, while the TW effect makes only a minor contribution to the equatorial warming as well as its seasonal evolution.

The GW-induced seasonal evolution of MLT and wind anomalies in the tropical Pacific differs from that of El Niño on many aspects. Under GW, the anomalous westerly propagates westward from the eastern to central equatorial Pacific during July of year 0 to January of year 1 (Fig. 4d). In response to the wind stress change, the maximum warming signal is also found to propagate correspondingly (Fig. 4b). The overriding experiments help isolate the role of individual feedback for the warming and its propagation. Over the CEP region (Fig. 5b), the most striking feature is that the seasonal variation of the MLT due to the WS effect

is just the opposite to that due to the TW effect (their correlation $r = -0.53$), e.g., the WS-induced warming reaches a minimum during boreal winter when the warming resulting from the TW effect happens to be a maximum. Their combined effects lead to small seasonal variation amplitude over the CEP region. This seasonal MLT analysis described above complements the work by Luo et al. (2015). They focused on the annual mean response in the tropical Pacific to GW and found that only 20 % of the annual warming in the eastern equatorial Pacific can be attributed to the WS effect. The analysis here, on the other hand, indicates that the WS effect is important in the seasonal evolution of the MLT response to GW in the equatorial Pacific.

ENSO events tend to peak during boreal winter and can be viewed as a disruption of the seasonal cycle (Fig. 4a). It can be seen that GW projects even more strongly on to a weakening of the seasonal cycle of the MLT, expressed as greater warming during cold months (boreal winter) in the CEP (Fig. 4b; the pattern correlation between anomalous

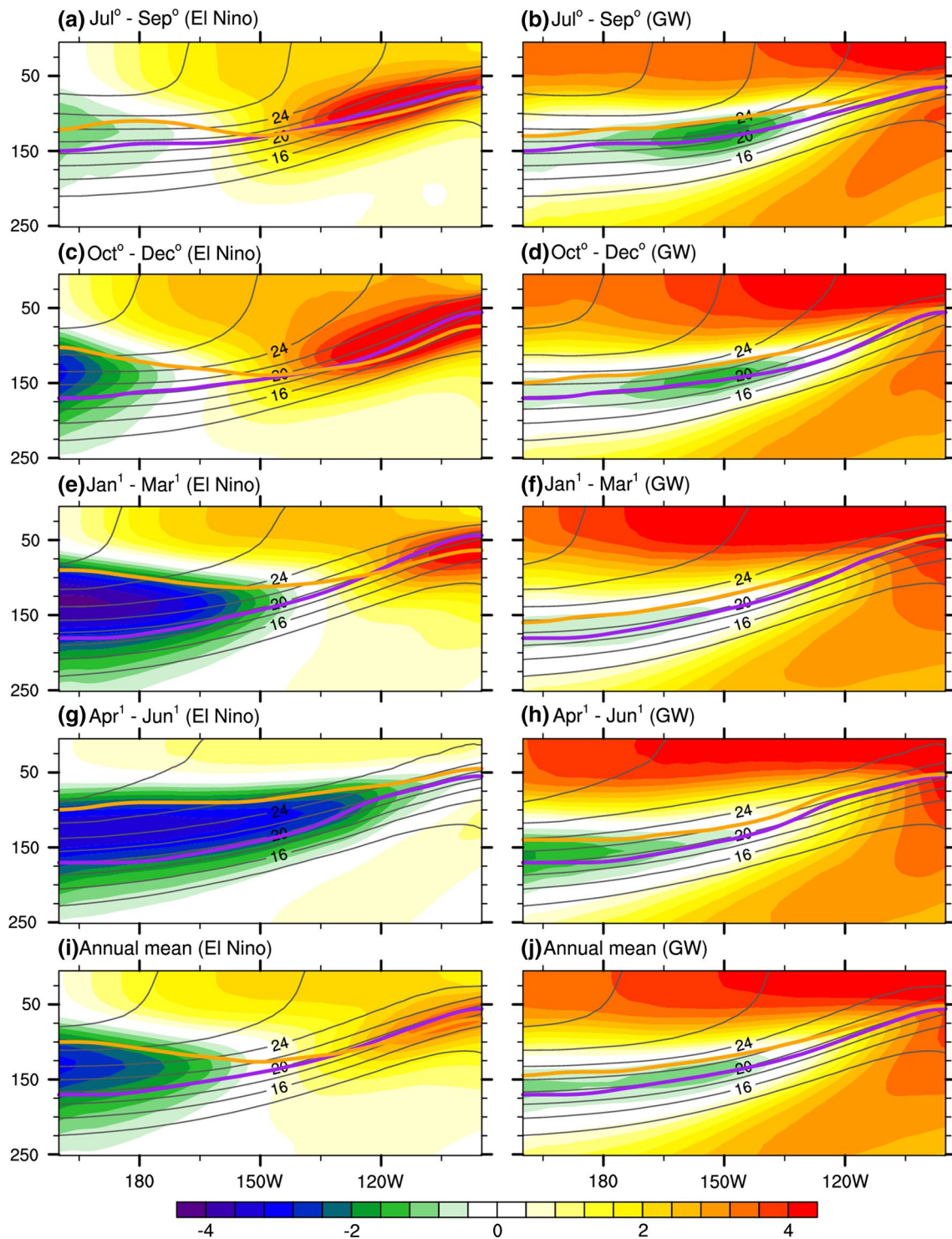


Fig. 6 Seasonal evolution of temperature anomalies (*shading*) and their corresponding climatological fields (*black contours*) along the equator (averaged between 2.5°S and 2.5°N) during the El Niño composite (*left*) and GW (*right*). Superimposed are the thermocline depths (*thick purple lines* from an average of 2006–2025; *thick yellow*

lines on the left-hand side panels from an average of the 18 El Niño composite members, and *thick yellow lines* on the right-hand side panels from an average of 2080–2099). The thermocline depth is identified as the location of the maximum vertical gradient of temperature

and mean MLT is -0.73). Note that the response of the seasonal cycle of the tropical Pacific SST to global warming could be model-dependent. For example, Jia and Wu (2013) found an enhanced seasonal cycle of SST in the equatorial Pacific in response to GW in a simple coupled model, while Zelle et al. (2005) found no obvious changes in the SST seasonal cycle from an earlier version of the community climate model.

Notwithstanding the model sensitivity, our overriding experiments help to identify the source of the change of the seasonal cycle in MLT: its reduction during El Niño is dominated by WS effect (Fig. 5a), while that under GW is resulted from the superposition of the WS and TW effects (Fig. 5b). In addition to the MLT, under GW, significant negative pattern correlations are also found over the CEP for other near-surface variables between their mean and anomalous fields (-0.90 for zonal wind stress, -0.45 for vertical velocity, and -0.59 for mixed layer stratification, respectively), indicating notable reductions in their seasonal cycle that are strongly phase-locked to the mean seasonal cycle (Fig. 4d, h, j). In comparison, their reductions during El Niño are less phase-locked. Take vertical velocity for example, the GW-induced downwelling reaches a maximum during boreal winter when the climatological vertical velocity happens to be largest upward, while the downwelling induced by El Niño is about 2 months earlier and is somewhat westward shifted (Fig. 4g, h).

4.3 Subsurface changes

Substantial differences between El Niño and GW are also found at the subsurface in the equatorial Pacific. CESM reproduces well the major features of the thermocline change in the tropical Pacific Ocean typical to El Niño (Wang and McPhaden 2000, 2001), including a shoaling in the west and a deepening in the east, i.e., in a form of a seesaw during much of the El Niño year (Fig. 6i). As the development phase of the El Niño cycle proceeds, a westerly wind anomaly (Fig. 4c) results in anomalous eastward current (Fig. 4e) and downwelling (Fig. 4g) east of 150°E through anomalous Ekman convergence, leading to positive temperature anomaly at subsurface and the deepening of the thermocline in the eastern Pacific. Then, this anomaly gradually amplifies and expands, and reaches a maximum in Oct.–Dec. of year 0 (Fig. 6c). During this process, a cold subsurface temperature anomaly also starts to develop in the western Pacific in order to compensate for upwelling and the eastward current near the surface, and the thermocline water further diverges and upwells, resulting in a significant cooling at subsurface and a shoaling of the thermocline in the decay phase of El Niño. This anomalous cooling gradually propagates eastward and upward to the eastern Pacific and replaces the warm anomaly during

demise phase, and then leads to a La Niña. As in the observations (Ohba and Ueda 2007), the penetration of the subsurface temperature anomaly appears in the form of an upwelling oceanic equatorial Kelvin wave, which is forced by the anomalous easterly winds over the western Pacific.

Under GW, however, the subsurface change is featured with an overall shoaling of the equatorial thermocline, with more shoaling in the central and west together with a cooling there (Fig. 6j). The shoaling of the thermocline in the east is resulted from a more stratified upper layer due to ocean warming that is greater near the surface and decreasing with depth (Luo et al. 2009), while the shoaling as well as the associated cooling in the central and west Pacific arise mainly from the WS effect (as found in Luo et al. 2015), which can be conveniently explained by the relaxation of the equatorial easterlies associated with the slowdown of Walker circulation (Vecchi and Soden 2007). Another difference from El Niño is that the seasonal evolution of the subsurface cooling in the equatorial Pacific cannot be characterized by a Kelvin wave propagation (right panels of Fig. 6). In stead, we find hints of westward propagation of upwelling Rossby waves off the equator under GW. In particular, associated with the summer cyclonic wind stress curl, there appear pronounced negative SSH anomalies developing over the east between 2.5° and 7.5°N , which travel westward in the form of oceanic upwelling Rossby waves (not shown).

4.4 Northward heat transport

Meridional heat transport is one of the most fundamental properties of the climate system (Hazeleger et al. 2004). Here we examine the changes in the annual mean northward heat transport (NHT) for the Pacific Ocean resulting from both El Niño and GW (Fig. 7). The climatological NHT appears to have a high degree of inter-hemispheric anti-symmetry with its sign reversed at the equator. Its peak values are 0.8 PW around 15°N and -0.9 PW around 15°S respectively, which are within the uncertainty range found by Trenberth and Caron (2001). This NHT dipole is believed to be associated with the shallow meridional overturning circulation (MOC) in the Pacific (McPhaden and Zhang 2002), i.e., the Subtropical Cells (STCs; McCreary and Lu 1994) and its equatorial components, the TCs (Perez and Kessler 2009). While the TCs takes surface water away from the equator and then recirculates vertically within the tropics, the STCs transports warmer water out of the tropics within the surface layer and brings colder water from the subtropics back to the equator in the thermocline (contours in Fig. 8).

During El Niño, it is found that the NHT in FULL (Fig. 7a) increases greatly in the tropics from 10°S to 20°N , with the maximum of ~ 0.9 PW at 7°N , and decreases north

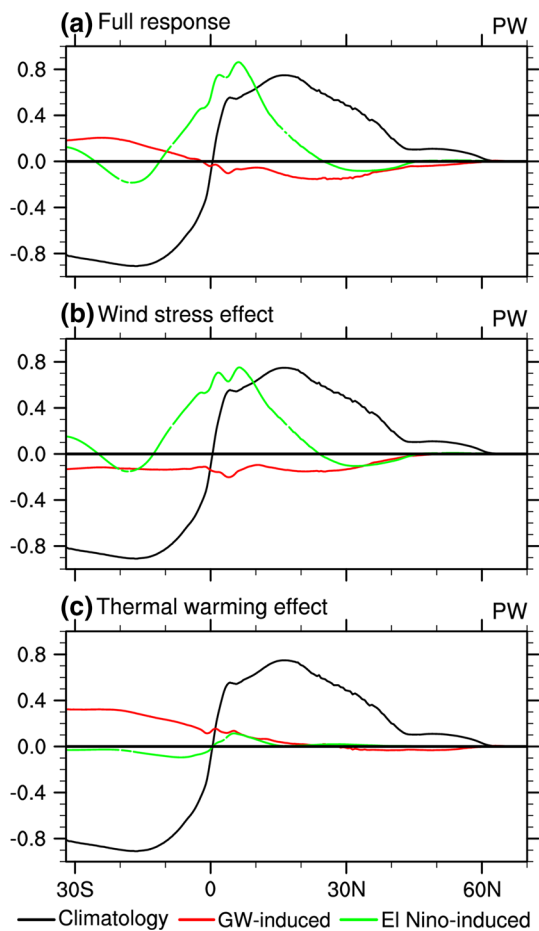


Fig. 7 The El Niño- (green) and GW-induced (red) Pacific northward heat transports (NHT) in **a** full response (FULL-CTRL), **b** wind stress effect (FULL-STRS), and **c** thermal warming effect (WIND-CTRL). Black lines are the climatological Pacific NHTs in CPL85

of 20°N and between 10°S and 30°S. The above response of the NHT is related to the changes in the Pacific shallow MOC during El Niño (Fig. 8a), i.e., the STCs both in the north and south appear to spin up but the TC in the south slows down significantly. The overriding experiments reveal that the El Niño-induced NHT change is due mainly to the WS effect (Fig. 7b), which is further confirmed by the MOC response to the WS change during El Niño (Fig. 8c).

Under GW, however, it is found that the response of the NHT is not so significant in comparison with El Niño, and appears to be anti-symmetric about the equator with a decrease in the northern hemisphere but an increase in the southern hemisphere (Fig. 7a). This change of the NHT represents a reduction of the poleward transports in both hemispheres, which is again consistent with the symmetric change in MOC that appears to be weakened in both hemispheres under GW (Fig. 8b). According to the overriding experiments, the reduction in the north is due mainly to the

weakened trade winds (not shown) which significantly suppress the northward Ekman transports (Fig. 8d), while the reduction in the south is mainly driven by the upper-ocean density changes (not shown) induced by the TW effect (Fig. 8f).

The GW-induced reduction of the poleward heat transport in the tropical Pacific would induce a net heating to the atmosphere, driving a stronger Hadley cell in the atmosphere (Feldl and Bordoni 2015). This might be the underlying mechanism for why overall the Hadley cell weakens more in the slab model simulation than in the climate models coupled with full ocean dynamics under increasing CO₂ forcing (Vecchi 2007, personal communication).

5 Analysis of mixed layer heat budget

In this section we analyze each term on the right hand side of Eq. (1) and examine their responses to El Niño versus GW, respectively. Figure 9 shows the annual-mean forcing terms for the tendency of MLT during El Niño and GW. It is found that there are substantial differences on the major balance terms as well as their roles that maintain the warming in the CEP. During El Niño, they are vertical advection (warming), net heat flux (cooling) and diffusion (cooling). Under GW, however, the most prominent terms in the balance are the cooling from vertical advection and warming from diffusion. More details are discussed below.

5.1 Vertical advection

In agreement with previous observational studies of the ENSO cycle (e.g., Wang and McPhaden 2000, 2001), the reduction of cold vertical advection plays a critical role for the anomalous surface warming in the CEP (Fig. 9a), dominating the development and decay of El Niño events (compared Fig. 10a with c). More specifically, the anomalous vertical advection is resulted from weakening of both stratification (Fig. 12a) and vertical velocity (Fig. 12c), with the former playing a larger role in the east and the latter in the central equator. The weakening of the vertical velocity is due to anomalous Ekman convergence from the reduction of the surface easterly, while the weakening of the stratification is due to the deepening of the thermocline. However, both changes are resulted from the weakened easterlies along the equator. This is confirmed by the overriding experiments, which reveals that the WS change dominates overwhelmingly the magnitude and seasonal evolution of the vertical advection while the TW effect tends to damp the effect from the WS change (Fig. 11c).

In sharp contrast, the response of the vertical advection to GW exerts a cooling effect on the surface layer over the CEP region (Fig. 9b). The cooling results from the

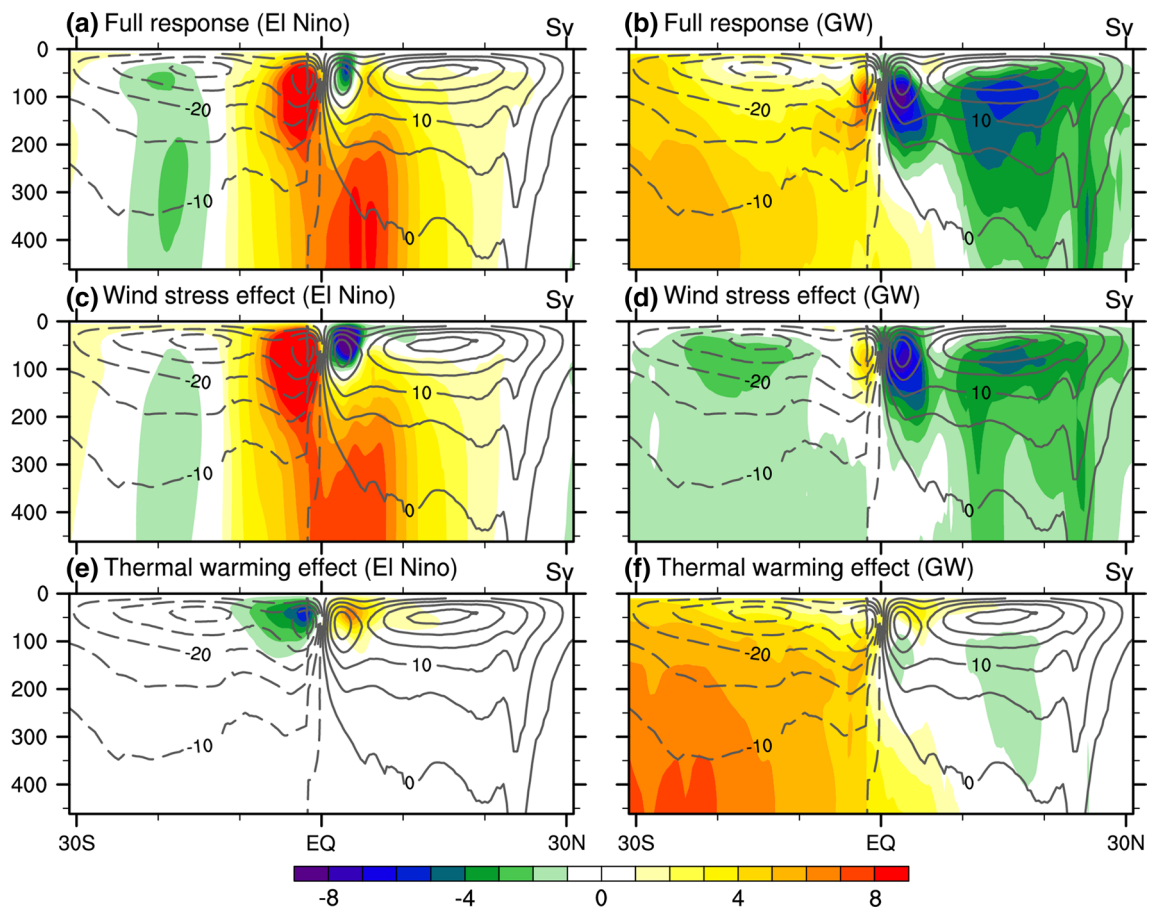


Fig. 8 The El Niño- (left) and GW-induced (right) changes (shading; Sv) in the Pacific meridional overturning circulation (MOC) and their climatological values (contours; Sv) in **a, b** full response (FULL-

CTRL), **c, d** wind stress effect (FULL-STRS), and **e, f** thermal warming effect (WIND-CTRL). Positive (negative) values indicate a clockwise (counterclockwise) circulation

significantly enhanced stratification (Fig. 12b), although the reduced vertical velocity induces a warming there (Fig. 12d). This result is in agreement with the finding of DiNezio et al. (2009). Through analyzing 11 CMIP3 climate models, they found that greenhouse gas forcing results in an anomalous vertical advective cooling in the eastern equatorial Pacific, resulting mainly from the significantly enhanced near-surface thermal stratification in spite of the existence of weakened upwelling. The important controlling role of the stratification for the vertical advection is further confirmed by its seasonal evolution, i.e., the vertical advection (Fig. 10d) evolves synchronously with the stratification (Fig. 4j). The overriding experiments further reveal that, unlike El Niño, both the WS and TW effects are important in shaping the seasonal cycle of the CEP response to GW (Fig. 11d).

5.2 Zonal advection

Our analysis indicates that El Niño induces a warming anomaly of the zonal advection in the western and central

equatorial Pacific but a cooling anomaly in the east equatorial region (Fig. 9c). This result is in agreement with the modeling work by Huang et al. (2012) but with different mechanism. In our analysis, the warm zonal advection over the western and central equatorial Pacific is resulted from the decrease of both zonal surface current and temperature gradient associated with the weakened easterlies, while the cooling over the east is mainly due to the anomalous westward zonal currents there (Fig. 12e, g). However, in Huang et al. (2012), the enhanced zonal temperature gradient plays a dominant role in the cooling over the eastern equatorial Pacific. Nevertheless, the anomalous zonal advection is a major warming term in the western Pacific and its seasonal evolution is in phase with the evolution of T_r (compared Fig. 10e-a), indicating its important role in the surface heat balance there, which is consistent with previous studies (McPhaden and Picaut 1990; Picaut and Delcroix 1995; Picaut et al. 1996). In addition, the zonal advection mainly contributes to the decay and demise phases of El Niño over the CEP (Fig. 11e), indicating its importance to the transition of ENSO phase. The

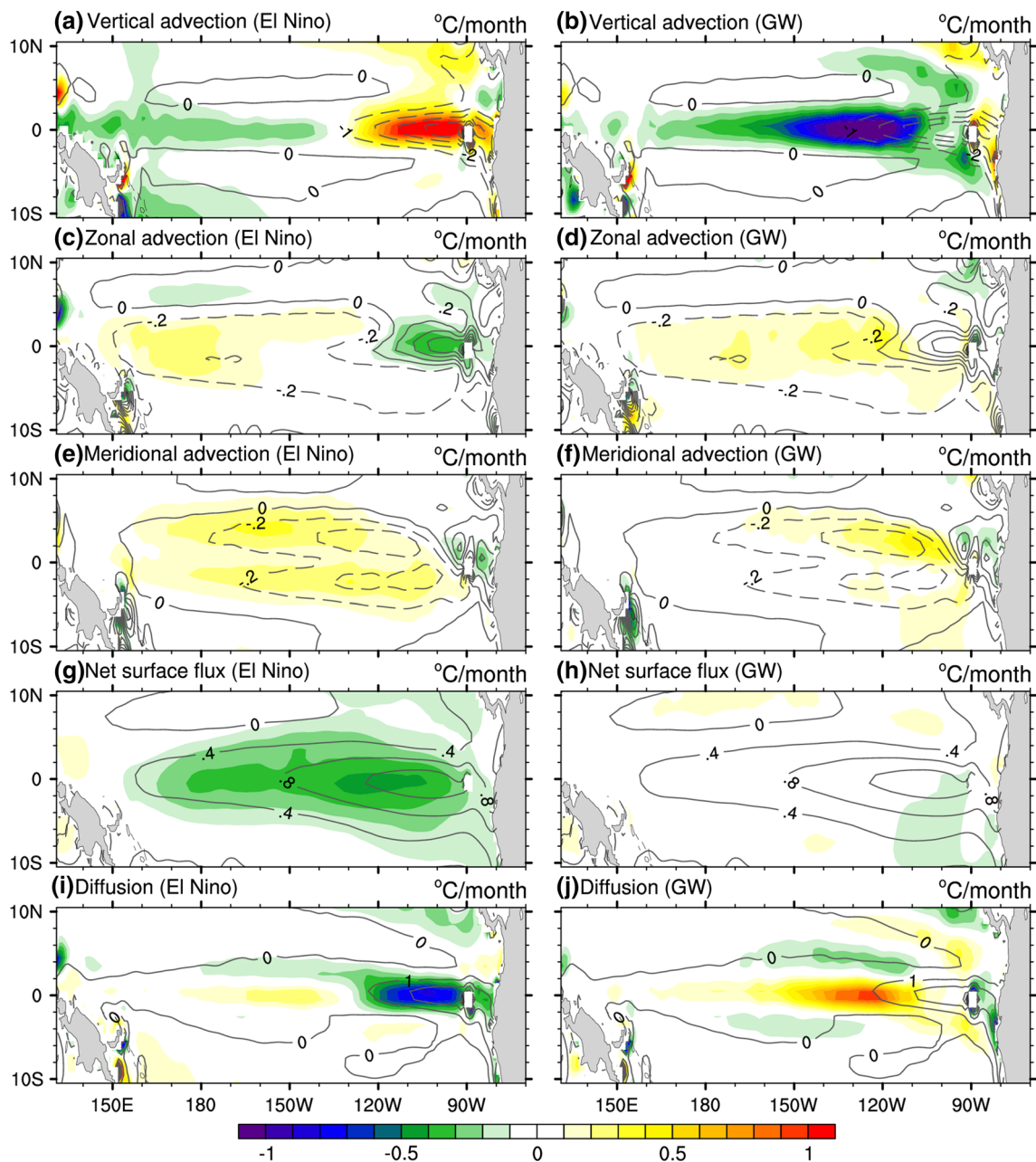


Fig. 9 The El Niño- (left) and GW-induced (right) changes (shading) and their corresponding climatological fields (contours) in the heat budget terms during the “El Niño year”: **a, b** vertical advection, **c, d**

zonal advection, **e, f** meridional advection, **g, h** net surface heat flux, and **i, j** diffusion

overriding experiments further confirm the evolution of the anomalous zonal advection in the CEP is dominated by the WS change (Fig. 11e).

The changing pattern of the zonal advection in the western and central Pacific under GW (Figs. 9d, 10f) is similar to what happens during the peak phase of El Niño (Figs. 9c, 10e). However, different from the situation during El Niño, the anomalous zonal advection brings a warming effect over the eastern equatorial region, which is due

mainly to the weakened zonal current (Fig. 12h) while the contribution from the zonal temperature gradient is negligible (Fig. 12f). In addition, the overriding experiments show that the zonal advection in the CEP under GW (Fig. 11f) is substantially modulated by the TW effect compared to that under El Niño (Fig. 11e). In the former, the anti-correlation ($r = -0.65$) between the WS- and TW-induced changes in zonal advection indicates a cancellation between these two effects.

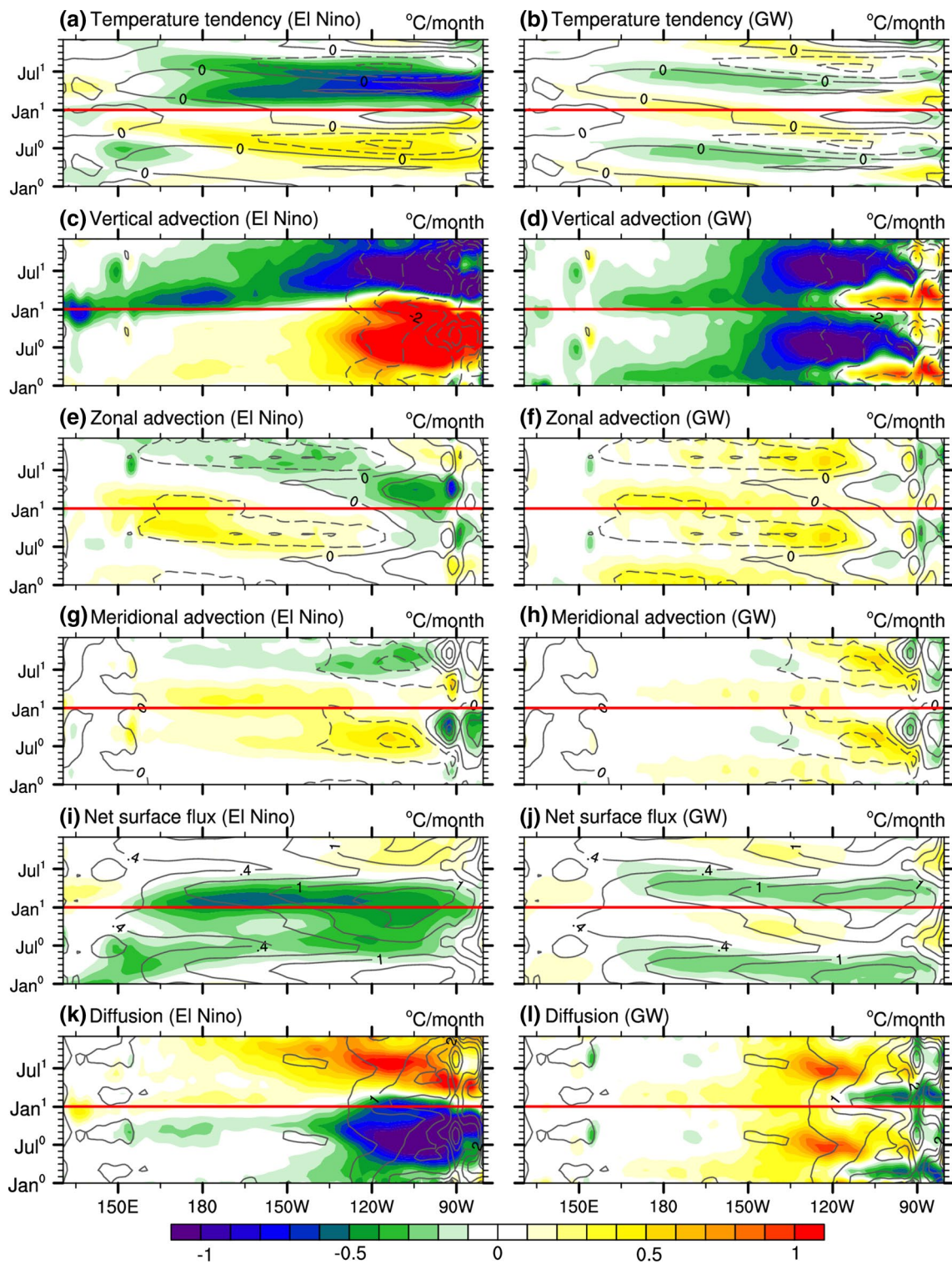


Fig. 10 Seasonal evolution of changes (*shading*) and their corresponding climatological fields (contours) in the heat budget terms during El Niño (*left*) and GW (*right*) along the equator (averaged

between 2.5°S and 2.5°N) **a, b** temperature tendency, **c, d** vertical advection, **e, f** zonal advection, **g, h** meridional advection, **i, j** net surface heat flux, and **k, l** diffusion

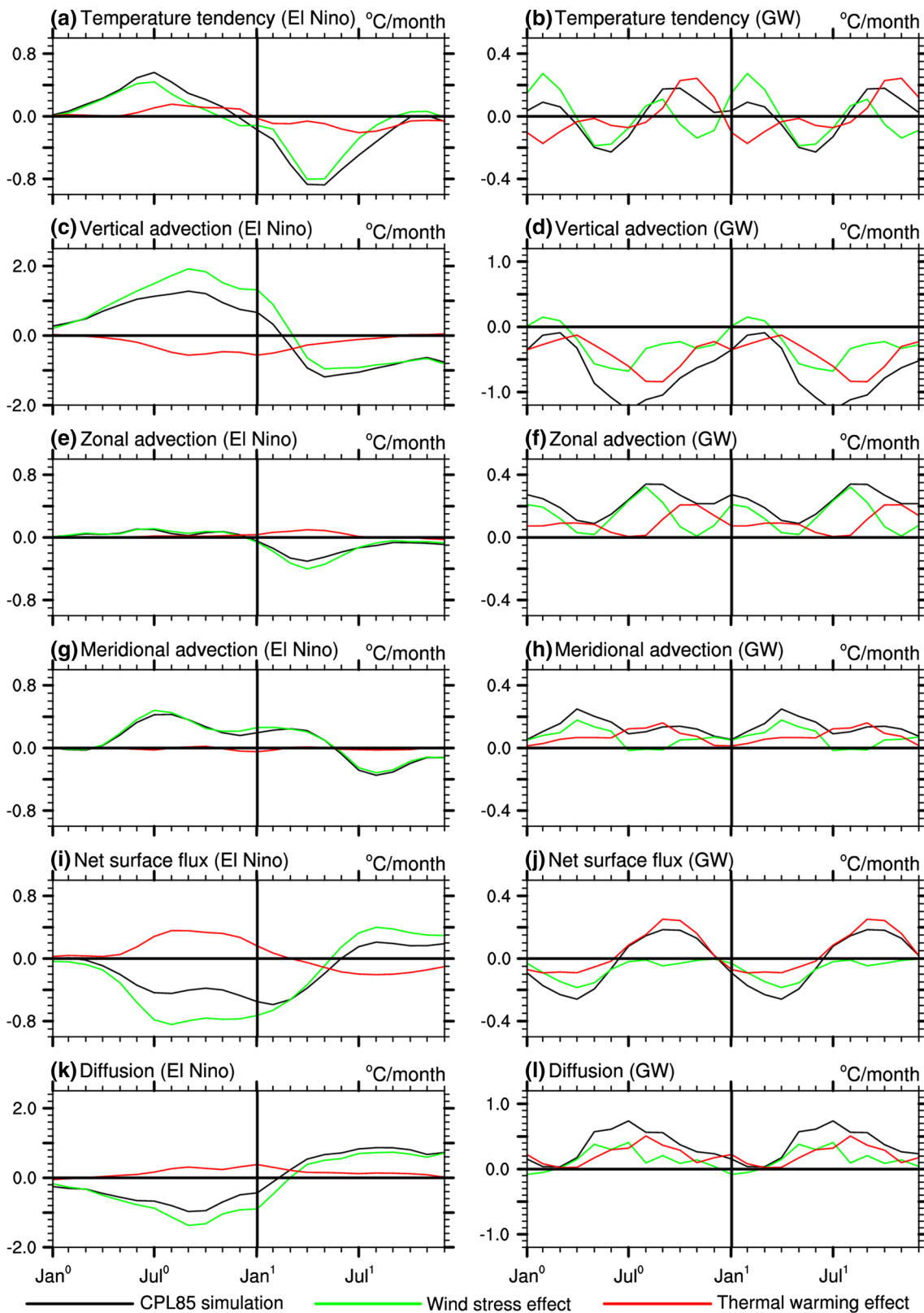


Fig. 11 The El Niño- (*left*) and GW-induced (*right*) changes over the CEP in **a, b** temperature tendency, **c, d** vertical advection, **e, f** zonal advection, **g, h** meridional advection, **i, j** net surface heat flux, and **k,**

l diffusion from CPL85 simulation (*black*), wind stress effect (FULL-STRS) (*green*), and thermal warming effect (WIND-CTRL) (*red*)

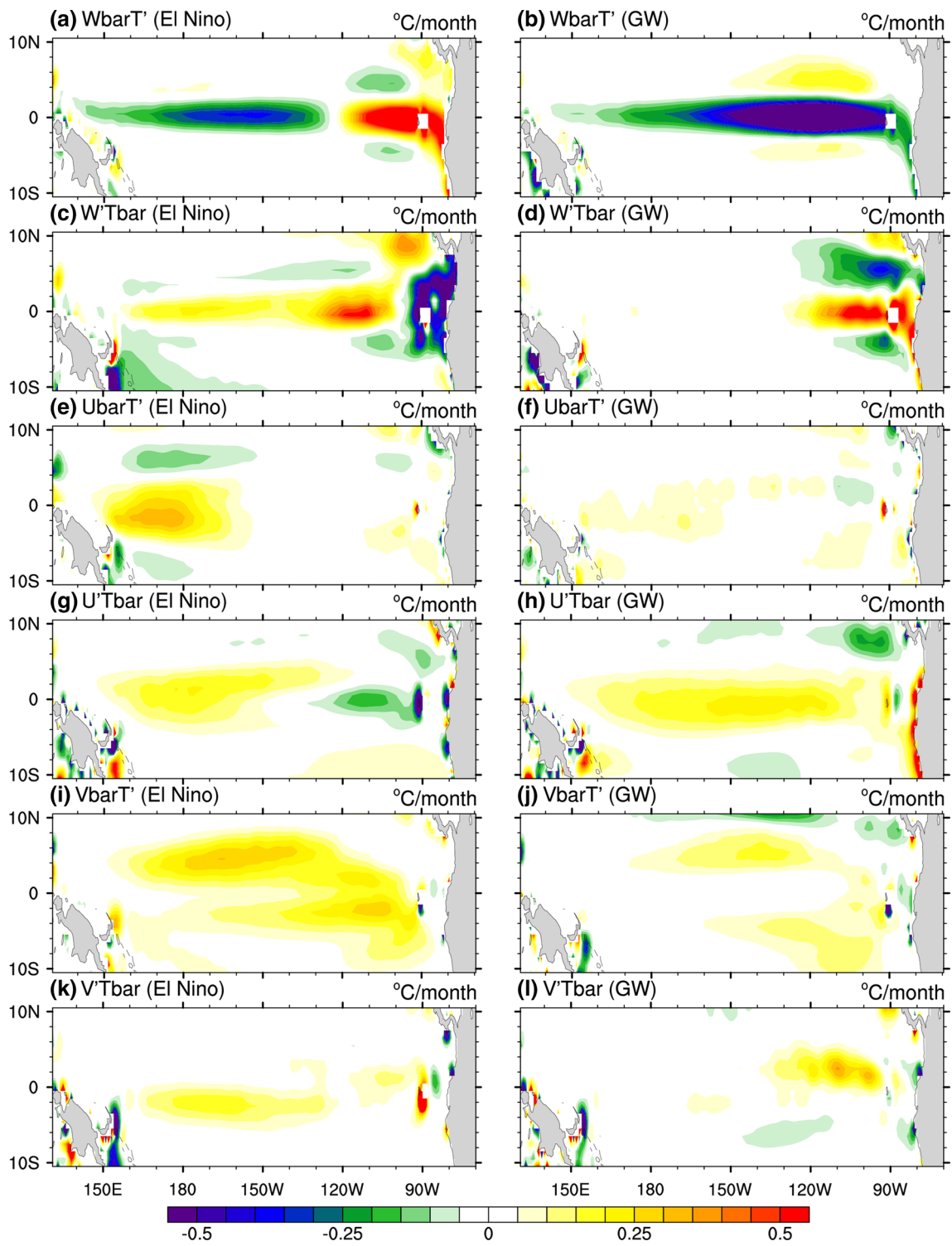


Fig. 12 The El Niño- (left) and GW-induced (right) temperature budget distributions **a, b** $-w'T'_z$, **c, d** $-w'T'_z$, **e, f** $-u'T'_x$, **g, h** $-u'T'_x$, **i, j** $-v'T'_y$ and **k, l** $-v'T'_y$

5.3 Meridional advection

The meridional advection also contributes to the formation and decay of the El Niño, especially in the central Pacific (Fig. 10g). During the development phase of El Niño, the cooling effect of the meridional advection is reduced, and the maximum reduction appears a few degrees latitude off the equator over the CEP region (Fig. 9e), resulting mainly from weakening of the meridional temperature gradients (Fig. 12i) associated with the enhanced equatorial SST, with the Ekman divergence (Fig. 12k) associated with the weaker easterlies making a minor contribution. Figure 10g shows that the anomalous meridional advection contributes to the developing and decay phases over the CEP region. The overriding experiments further reveal the dominant role of the WS change in the anomalous meridional advection during El Niño (Fig. 11g).

GW also leads to a warming anomaly of the mean meridional advection with its maxima a few degrees off the equator. However, their locations move eastward (Fig. 9f) in direct response to the eastward shift of the weakened easterlies relative to that of El Niño. Under GW, in addition, the anomalous meridional advection appears to be a warming source to the eastern Pacific and plays a more significant role for the heat balance there than the anomalous zonal advection (Figs. 9f, 10h). The meridional advective warming over the CEP is resulted mainly from the weakening of the poleward current (Fig. 12l), in contrast to the situation during El Niño in which the weakening in the meridional temperature gradient plays a more important role (Fig. 12j). The overriding experiments reveal that both the WS and TW effects may work cooperatively to drive the changes in meridional advection under GW (Fig. 11h).

5.4 Net heat flux

During El Niño, the net heat flux is significantly reduced over the CEP region (Fig. 9g) and this change acts to damp the El Niño development (Fig. 10i), similar to the observations (Wang and McPhaden 2000, 2001). We further decompose the net heat flux into latent heat flux (LHF), sensible heat flux (SHF), longwave radiation (LR) and shortwave radiation (SR). It can be seen from Fig. 13 that during El Niño the heat flux change along the equator is mainly contributed by changes in the LHF and SR. This is in agreement with previous studies (e.g., Wang and McPhaden 2000; Zhang et al. 2007; Huang et al. 2010). In particular, the negative LHF in the CEP region (Fig. 13a) is resulted from the increased evaporative cooling associated with the anomalous warming surface ocean (Zhang et al. 2007), while the reduced SR in the central and western equator (Fig. 13g) is due mainly to the increased cloudiness (Lloyd et al. 2012). Changes in SHF and LR (Fig. 13c, e)

are almost negligible compared to the other two terms. Our overriding experiments suggest that the TW effect warms the CEP during El Niño, acting to reduce the cooling from the WS effect (Fig. 11i). This exemplifies the active role of the wind-driven ocean dynamics in the surface energetics of the ENSO life cycle.

In contrast to the remarkable reduction of the net heat flux during El Niño, GW induces much weaker annual mean change in the net heat flux (Fig. 9h), which is partly due to a cancellation between the heating during Jul.–Nov. and the cooling during Dec.–Jun. (Fig. 10j). The negligible change of the net heat flux over the CEP is due to a reduction of both SR (Fig. 13h) and LR (Fig. 13f), with the former resulting from increased cloudiness and the latter from more infrared energy flux trapped by the increased atmospheric CO₂. In addition, GW-induced LHF anomalies in the central equator are rather small (Fig. 13b), in contrast to the large LHF there during El Niño. On the other hand, the net heat flux over the WEP does not change much (Fig. 9h) due to the balance between reduced net upward longwave radiation (Fig. 13f) and enhanced heat loss by evaporation (Fig. 13b). This supports the result by Knutson and Manabe (1995) who found that increasing CO₂ induces more latent heat cooling in the west than east. The overriding experiments reveal that the thermal warming acts to inject warming into the CEP region by average while the WS effect acts to extract heat from the ocean (Fig. 11j). Unlike other ocean circulation related budget terms, the evolution of net heat flux response is clearly dominated by TW effect, which can be attributed to the dominant role of air-sea thermal interaction in regulating the heat flux under GW.

5.5 Diffusion

During El Niño, the diffusive warming in the CEP is significantly decreased (Fig. 9i) and the resultant cooling anomaly acts to compensate the strong vertical advective warming there (Fig. 9a). This change in the diffusion may be explained as below. The ocean stability in the upper layer of the CEP is decreased due to the greater anomalous warming at subsurface than surface during El Niño (Fig. 6i). This stimulates the vertical diffusivity through a Richardson number-dependent parameterization (Pacanowski and Philander 1981), and this warm diffusive flux and entrainment in turn lead to an anomalous cold vertical diffusion (e.g., Yang et al. 2009). Seasonally, the diffusive cooling reaches the maximum during the peak phase of El Niño over the CEP (Fig. 10k), and its seasonal variation is mainly controlled by the WS effect (Fig. 11k).

Under GW, in stark contrast to El Niño, the anomalous diffusion is a warming effect in the CEP (Fig. 9j), compensating the vertical advective cooling there (Fig. 9b). The diffusive warming is resulted from greater warming in the

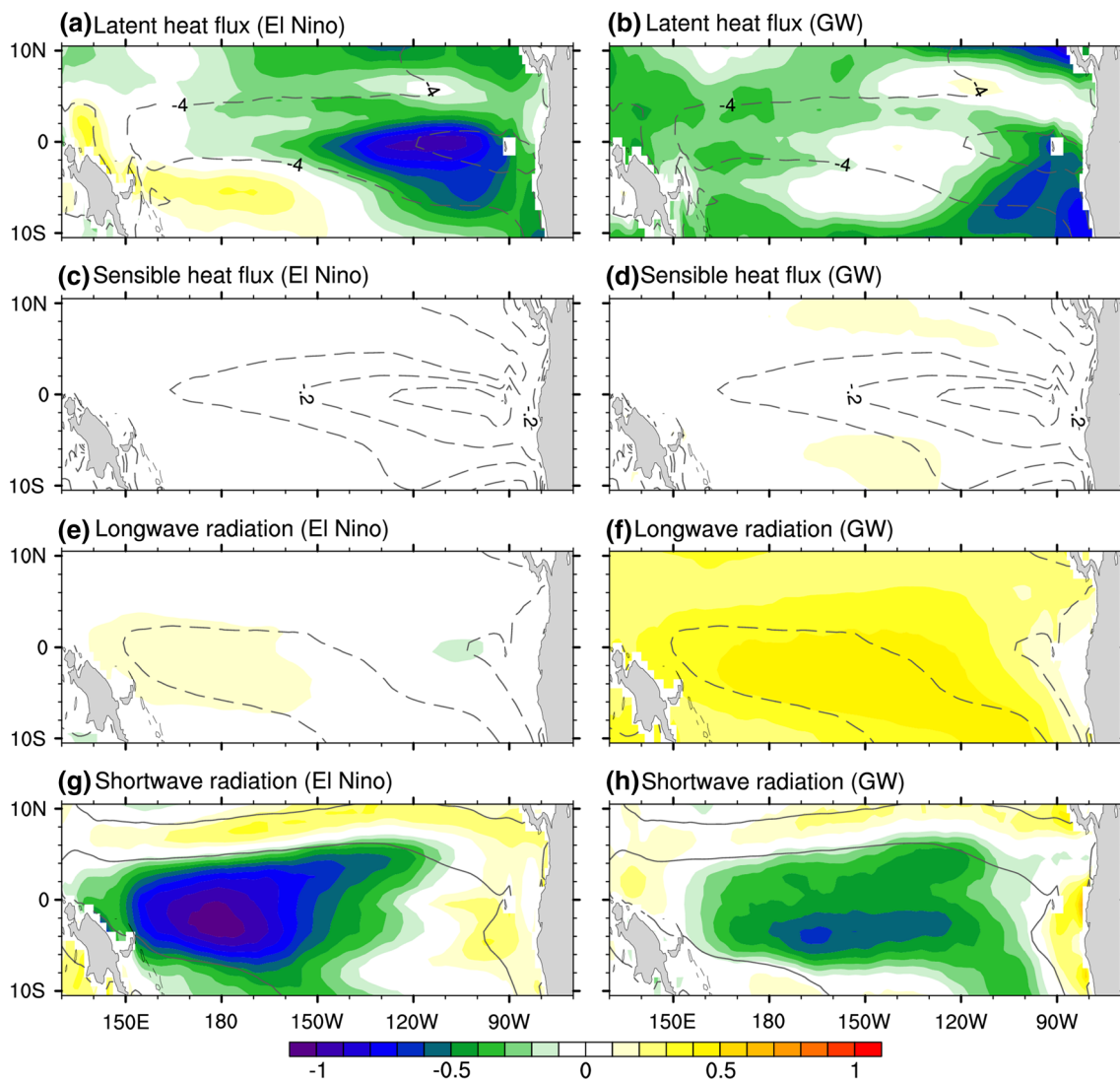


Fig. 13 The El Niño- (*left*) and GW-induced (*right*) changes (*shading*) and their corresponding climatological fields (contours) during the “El Niño year”: **a, b** latent heat flux, **c, d** sensible heat flux, **e, f** longwave radiation, and **g, h** shortwave radiation

surface than subsurface under GW, opposite to what happens during El Niño as being explained in the last paragraph. This compensation relationship between the diffusion and the vertical advection in our model is further verified by their seasonal evolution (Fig. 10d, l), that is, when the anomalous vertical advective cooling reaches its maximum over the CEP during the boreal summer, the anomalous diffusive warming also appears to be a maximum. In addition, the overriding experiments reveal that the changes in the diffusion under GW are due to a combination of both the WS and the TW effects (Fig. 11l).

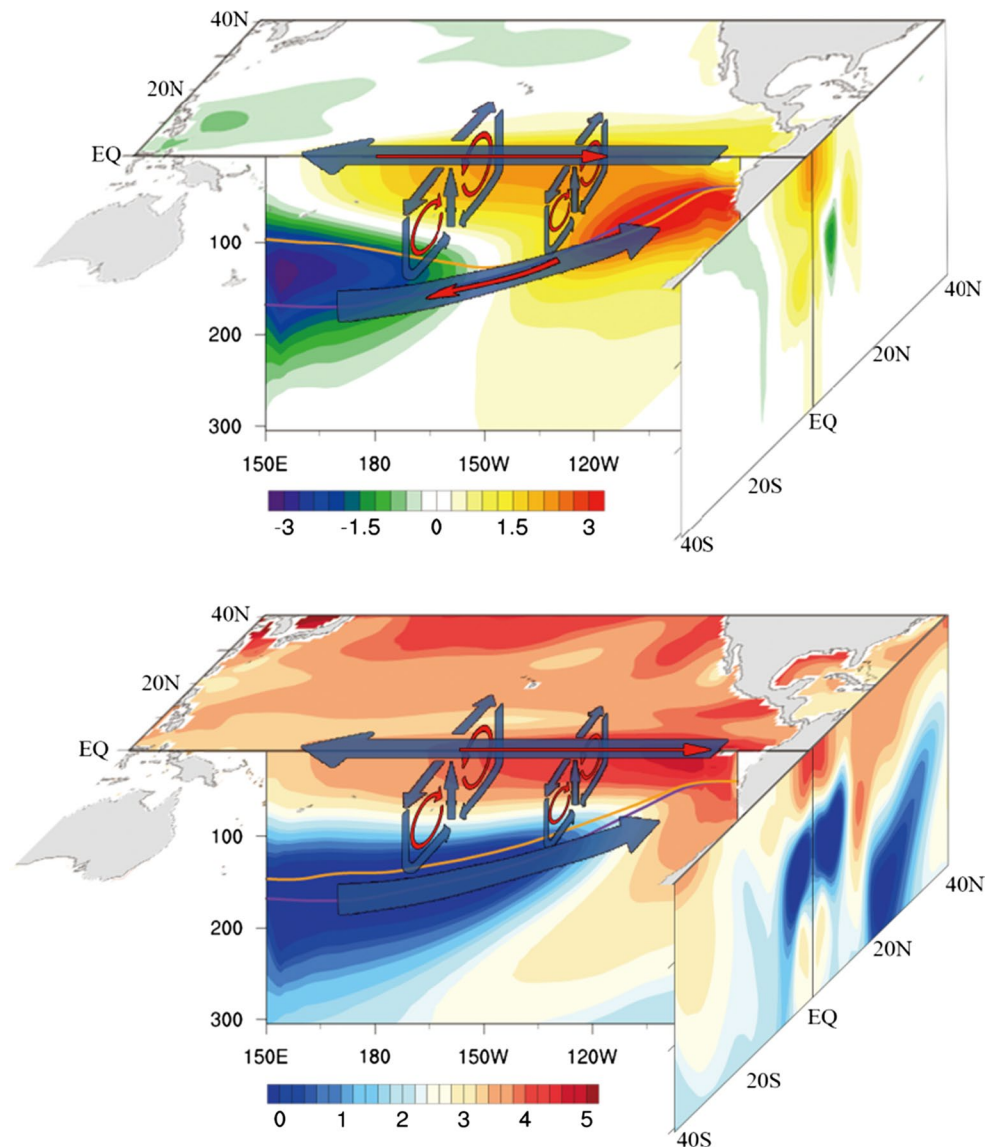
Our above result of the heat budget analysis under GW is roughly in agreement with Jia and Wu (2013), whose analysis were based upon an intermediate climate model with a full atmospheric general circulation model coupled to a 1.5-layer reduced-gravity ocean model. For example, they

also found that anomalous horizontal advection contributes to the warming in the central and eastern Pacific and a total contribution of changes in vertical advection and horizontal diffusion (comparable to the total contribution of vertical advection and diffusion in our model) is to cool the CEP region. However, there is a difference regarding the role of net surface heat flux change: it contributes to the warming in their model, while the annual mean contribution of the surface net flux is a weak cooling in our model.

6 Summary and discussion

There is increasing evidence that climate models tend to produce an El Niño-like sea surface response in the tropical Pacific under the forcing of increasing concentration

Fig. 14 Schematic depicting the changes for El Niño (*top*) and GW (*bottom*). *Color shading* indicates temperature anomalies at the sea surface (Northern Hemisphere only), along 140°W in the latitude-depth sense, and along the equator in the longitude-depth plane (averaged between 2.5°S and 2.5°N). Superimposed are the thermocline depths similar to those in Fig. 6i and j. *Bold* and *thin arrows* represent the mean and anomalous circulation



of greenhouse gases. However, through a GW-El Niño inter-comparison analysis, we find that many of the GW response features in the ocean as well as the related maintaining mechanisms turn out to be quite different from a typical El Niño. As summarized in Fig. 14, the major similarities and differences for the annual mean response are:

1. Both El Niño- and GW-induced patterns are featured with weakened equatorial trade winds. In response to the slowdown of the trade winds, there appears to be weakening in zonal SEC and meridional STC, enhancements in surface warming over the CEP and shoaling of thermoclines in the WEP.
2. Associated with the eastward shift of the weakened easterlies, the surface-warming center moves eastward and the weakening of the SEC are more significant in the CEP under GW in contrast to El Niño.
3. Over the CEP region, GW induces greater warming in the surface than subsurface while it is the other way around during El Niño. Taken together, GW-induced response is characteristic more of an enhanced stratification in the upper ocean than a shallower thermocline, whereas El Niño corresponds to a weaker upper ocean stratification and a deeper thermocline.

By implementing a suite of numerical experiments, this study has focused on identifying the similarities and differences of their seasonal evolution as well as examining the underlying formation mechanisms in the tropical Pacific between GW and El Niño. In spite of sharing some similarities between the two scenarios, many significant distinctions under GW from El Niño are found and summarized as below:

1. The GW-induced surface warming propagates from the eastern to central Pacific during Jul.–Dec. when the El Niño-induced surface warming propagates eastward characterized by a downwelling equatorial Kelvin wave.
2. The upper ocean of the CEP is less stratified during the entire El Niño year with the maximum on its peak phase in winter while the GW-induced stratification is weakened in Jan-Mar and then strengthened the rest of the year.
3. There are an overall reduction in the amplitude of the seasonal cycle of the MLT under both El Niño and GW. However, the reduction of the seasonal cycle is closely phase-locked with the background mean seasonal cycle for the case of GW and manifested in both the equatorial wind and the wind-driven upper ocean circulation (such as zonal wind stress, vertical velocity and mixed layer stratification).
4. In contrast to the penetration of the equatorial subsurface temperature anomaly that appears to propagate in the form of an oceanic equatorial Kelvin wave during El Niño, the GW-induced subsurface temperature anomaly propagates in the form of upwelling Rossby waves.
5. In the context of the designed overriding experiments, the WS effect is responsible for the evolution of El Niño, while the oceanic response to GW is due to a combination of both the WS change and the TW effect, with the former making a larger contribution to the seasonal cycle and the latter to the annual mean warming.
6. The integrated NHT also exhibits distinct characters between El Niño and GW in the tropical Pacific. The wind stress anomalies associated with El Niño drive across-equatorial cell between 10°S and 20°N, which transports net heat northward across the equator. However, the GW-induced reduction of the poleward oceanic heat transport is overall symmetric, with little cross-equatorial component.
7. During El Niño, the vertical advection associated with a weakening of both stratification and upwelling is clearly the dominant player although the horizontal advection also contributes in the central regions, while the net surface flux and the diffusion play a damping role. Under GW, however, it is the diffusion that makes a major contribution to the warming over the CEP, while the vertical advection associated with the strengthened stratification damps the warming there.

To further validate the results here based on our own CESM run (i.e., the CPL85), three members of RCP8.5 simulations with CESM are also obtained from NCAR. All the features regarding El Niño and GW found from the CPL85 run are replicated and confirmed with the NCAR

ensemble simulations (now shown), suggesting that our modeling approach is reliable for examining the oceanic response in the tropical Pacific to GW.

While the projected seasonal mean changes in the eastern Pacific (i.e., an El Niño-like warming pattern) are largely consistent among different climate models, the changes in the ENSO statistics are quite different. A recent study by Cai et al. (2014) suggested that, although the total number of El Niño events does not appear to have a significant change due to GW, the frequency of extreme El Niño events will increase substantially. Interestingly, our CPL85 simulation seems to corroborate this notion (Fig. 1). If an extreme El Niño event is defined as the MLT anomaly at Niño3.4 region exceeding 3.0 °C during the peak phase, its frequency is found to double from about one event every 23 years during the first half of the 21st century (2 events from 2006 to 2052) to one every 12 years during the second half of the 21st century (4 events from 2053 to 2099). The increase of extreme El Niño events have further been confirmed through the three ensemble members conducted by NCAR, in which the number of extreme El Niño events increases from 6 in the first half of 21st century to 12 in the second half of 21st century. Furthermore, Li et al. (2016) pointed out that the projected El Niño-like warming pattern and resultant increased frequency of extreme El Niño events are even underestimated, given that most models produce a cold tongue SST cooler than observations (Li and Xie 2012, 2014; Li et al. 2015). This increase may be associated with the El Niño-like mean warming response under GW, i.e., more surface warming in the CEP than the surrounding ocean waters, facilitating more occurrences of maximum SSTs, and hence convection for a given SST anomaly (Cai et al. 2014). This might also be linked to the reduction in the amplitude of the seasonal cycle, which usually implies a strong El Niño, because when less energy is within the seasonal cycle, more is left for inter-annual signal (Fedorov and Philander 2001; Guilyardi et al. 2009).

The result that the WES feedback on the SST changes in the Pacific is negligible should be taken with caution, for the key influence of WES on the southeastern Pacific SST is robust across the CMIP3 and CMIP5 climate models (e.g., Ma and Xie 2013; Li and Xie 2014). The cause of the underestimate of the WES feedback may lie in prescribing the atmospheric conditions in our ocean-alone settings. Further experiments with the CESM in partially coupled settings are underway to tease out the specific effects of WES in the SST response of the tropical Pacific to global warming.

Acknowledgments This work is supported by NSFC (41376009 & 41221063), NSF (AGS-1249173 & AGS-1249145), and the Joint Program of Shandong Province and National Natural Science Foundation of China (Grant No. U1406401). Y. Luo would also like to acknowledge the support from the Zhufeng and Taishan Projects of the Ocean

- Okumura YM, Ohba M, Deser C, Ueda H (2011) A proposed mechanism for the asymmetric duration of El Niño and La Niña. *J Clim* 24:3822–3829. doi:[10.1175/2011JCLI3999.1](https://doi.org/10.1175/2011JCLI3999.1)
- Pacanowski RC, Philander SGH (1981) Parameterization of vertical mixing in numerical models of tropical oceans. *J Phys Oceanogr* 11:1443–1451. doi:[10.1175/1520-0485\(1981\)011<1443:POVMIN>2.0.CO;2](https://doi.org/10.1175/1520-0485(1981)011<1443:POVMIN>2.0.CO;2)
- Perez RC, Kessler WS (2009) Three-dimensional structure of tropical cells in the central equatorial Pacific ocean*. *J Phys Oceanogr* 39:27–49. doi:[10.1175/2008JPO4029.1](https://doi.org/10.1175/2008JPO4029.1)
- Philip SY, van Oldenborgh GJ (2006) Shifts in ENSO coupling processes under global warming. *Geophys Res Lett* 33:1–5. doi:[10.1029/2006GL026196](https://doi.org/10.1029/2006GL026196)
- Picaut J, Delcroix T (1995) Equatorial wave sequence associated with warm pool displacements during the 1986–1989 El Niño-La Niña. *J Geophys Res* 100:18393
- Picaut J, Ioualalen M, Menkes C et al (1996) Mechanism of the zonal displacements of the Pacific warm pool: implications for ENSO. *Science* 274:1486–1489
- Picaut J, Masia F, duPenhoat Y (1997) An advective-reflective conceptual model for the oscillatory nature of the ENSO. *Science* 277:663–666. doi:[10.1126/science.277.5326.663](https://doi.org/10.1126/science.277.5326.663)
- Rasmusson EM, Carpenter TH (1982) Variations in tropical sea surface temperature and surface wind fields associated with the southern oscillation/El Niño. *Mon Weather Rev* 110:354–384. doi:[10.1175/1520-0493\(1982\)110<0354:VITSST>2.0.CO;2](https://doi.org/10.1175/1520-0493(1982)110<0354:VITSST>2.0.CO;2)
- Suarez MJ, Schopf PS (1988) A delayed action oscillator for ENSO. *J Atmos Sci* 45:3283–3287. doi:[10.1175/1520-0469\(1988\)045<3283:ADAOFE>2.0.CO;2](https://doi.org/10.1175/1520-0469(1988)045<3283:ADAOFE>2.0.CO;2)
- Trenberth KE, Caron JM (2001) Estimates of meridional atmosphere and ocean heat transports. *J Clim* 14:3433–3443. doi:[10.1175/1520-0442\(2001\)014<3433:EOMAAO>2.0.CO;2](https://doi.org/10.1175/1520-0442(2001)014<3433:EOMAAO>2.0.CO;2)
- Vecchi GA, Soden BJ (2007) Global warming and the weakening of the tropical circulation. *J Clim* 20:4316–4340. doi:[10.1175/JCLI4258.1](https://doi.org/10.1175/JCLI4258.1)
- Vecchi GA, Wittenberg AT (2010) El Niño and our future climate: where do we stand? *Wiley Interdiscip Rev Clim Chang* 1:260–270. doi:[10.1002/wcc.33](https://doi.org/10.1002/wcc.33)
- Wang W, McPhaden MJ (2000) The surface-layer heat balance in the equatorial Pacific Ocean. Part II: interannual variability*. *J Phys Oceanogr* 30:2989–3008. doi:[10.1175/1520-0485\(2001\)031<2989:TSLHBI>2.0.CO;2](https://doi.org/10.1175/1520-0485(2001)031<2989:TSLHBI>2.0.CO;2)
- Wang W, McPhaden MJ (2001) Surface layer temperature balance in the equatorial Pacific during the 1997–98 El Niño and 1998–99 La Niña. *J Clim* 14:3393–3407. doi:[10.1175/1520-0442\(2001\)014<3393:SLTBIT>2.0.CO;2](https://doi.org/10.1175/1520-0442(2001)014<3393:SLTBIT>2.0.CO;2)
- Wang C, Picaut J, (2004) Understanding ENSO Physics—A Review, in *Earth's Climate*. In: Wang C, Xie SP, Carton JA (eds) American Geophysical Union, Washington, DC. doi:[10.1029/147GM02](https://doi.org/10.1029/147GM02)
- Wang C, Weisberg RH (1994) On the “slow mode” mechanism in the ENSO-related coupled ocean-atmosphere models. *J Clim* 7:1657–1667
- Wang B, Zhang Q (2002) Pacific-East Asian teleconnection. Part II: how the Philippine Sea Anomalous anticyclone is established during El Niño development*. *J Clim* 15:3252–3265. doi:[10.1175/1520-0442\(2002\)015<3252:PEATPI>2.0.CO;2](https://doi.org/10.1175/1520-0442(2002)015<3252:PEATPI>2.0.CO;2)
- Weisberg RH, Wang C (1997) Slow variability in the equatorial West-Central Pacific in relation to ENSO. *J Clim* 10:1998–2017. doi:[10.1175/1520-0442\(1997\)010<1998:SVITEW>2.0.CO;2](https://doi.org/10.1175/1520-0442(1997)010<1998:SVITEW>2.0.CO;2)
- Xie S-P, Deser C, Vecchi GA et al (2010) Global warming pattern formation: sea surface temperature and rainfall*. *J Clim* 23:966–986. doi:[10.1175/2009JCLI3329.1](https://doi.org/10.1175/2009JCLI3329.1)
- Yang H, Wang F, Sun A (2009) Understanding the ocean temperature change in global warming: the tropical Pacific. *Tellus A* 61:371–380. doi:[10.1111/j.1600-0870.2009.00390.x](https://doi.org/10.1111/j.1600-0870.2009.00390.x)
- Zebiak SE, Cane MA (1987) A model El Niño-Southern oscillation. *Mon Weather Rev* 115:2262–2278. doi:[10.1175/1520-0493\(1987\)115<2262:AMENO>2.0.CO;2](https://doi.org/10.1175/1520-0493(1987)115<2262:AMENO>2.0.CO;2)
- Zelle H, Jan van Oldenborgh G, Burgers G, Dijkstra H (2005) El Niño and greenhouse warming: results from ensemble simulations with the NCAR CCSM. *J Clim* 18:4669–4683. doi:[10.1175/JCLI3574.1](https://doi.org/10.1175/JCLI3574.1)
- Zhang Y, Wallace JM, Battisti DS (1997) ENSO-like interdecadal variability: 1900–93. *J Clim* 10:1004–1020. doi:[10.1175/1520-0442\(1997\)010<1004:ELIV>2.0.CO;2](https://doi.org/10.1175/1520-0442(1997)010<1004:ELIV>2.0.CO;2)
- Zhang Q, Kumar A, Xue Y et al (2007) Analysis of the ENSO cycle in the NCEP coupled forecast model. *J Clim* 20:1265–1284. doi:[10.1175/JCLI4062.1](https://doi.org/10.1175/JCLI4062.1)
- Zhang Q, Guan Y, Yang H (2008) ENSO amplitude change in observation and coupled models. *Adv Atmos Sci* 25:361–366. doi:[10.1007/s00376-008-0361-5](https://doi.org/10.1007/s00376-008-0361-5)